Preferred citation: J-E. Gustafsson, V. Kaul and V. Lobosco. Densification and Dewatering in High Temperature Wet Pressing. In **The science of papermaking**, *Trans. of the XIIth Fund. Res. Symp. Oxford, 2001*, (C.F. Baker, ed.), pp 679–708, FRC, Manchester, 2018. DOI: 10.15376/frc.2001.1.679.

DENSIFICATION AND DEWATERING IN HIGH TEMPERATURE WET PRESSING

Jan-Erik Gustafsson, Vikram Kaul and Vinicius Lobosco

STFI, Swedish Pulp and Paper Research Institute
Box 5604, SE-114 86 Stockholm, Sweden

ABSTRACT

A number of quantitative models of wet pressing have been proposed in the literature but none of them take into account the observed rate dependence of the structural pressure. This rate dependence, which is ascribed to the flow resistance of the water in the fibre walls, should be incorporated in wet pressing models.

This paper presents a hydrodynamic model of wet pressing that includes the rate dependence of the structural pressure and thus takes into account the flow resistance of the intra-fibre water. The model is general in the sense that it can predict changes in the state of the fibre web due to a pressure pulse of arbitrary shape, under a wide range of web saturation and temperature conditions. The model can predict the effect of high press-roll temperatures.

The predictive capability of the model has been studied with the help of data from the third press of a pilot paper machine. For wet pressing at ambient temperatures, the model gives good predictions of solids content over wide ranges of machine speeds, grammages and linear loads and its predictive capability is quite adequate for most engineering applications.

For high press roll temperatures, the predictions are satisfactory over a wide range of press roll temperatures and linear loads but some significant systematic discrepancies occur. These predictions can probably be improved by using better estimates of the

hardening curves at high temperatures. Once calibrated, the model can give considerable information about changes in the state of the web as it passes through the nip and some insights about the mechanisms that are active.

INTRODUCTION

A large body of experimental studies and qualitative analysis has resulted in a broad consensus about the main mechanisms that are involved in the removal of water and compaction of the fibre web in wet pressing. MacGregor [1] presented a fairly comprehensive review of the literature available in 1989. Since then, Szikla [2], Burns et al. [3], Laivins and Scallan [4], Ahlman [5], Vomhoff [6], and Maloney [7] have reported new results from later studies.

In a wet web of fibres, water is located in pores between the fibres (extra-fibre water) and in the porous structure of the fibre walls (intra-fibre water). If a compressive force is applied to the wet fibre web, it compresses the fibre network and also creates a hydraulic pressure in the extra-fibre water. This hydraulic pressure causes some of the extra-fibre water to flow out of the web. Thus, at every point in a press nip, two component forces balance the applied force; one component due to the hydraulic pressure and the other due to the structural pressure (i.e. the resistance to deformation of the fibre network).

The average (Darcy) flow of extra-fibre water in modern press nips is primarily perpendicular to the plane of the web, towards the web surface(s) and into the water receiver, usually a felt. The extra-fibre hydraulic pressure decreases in the direction of flow and is a minimum at the permeable surface(s). Consequently there is also a gradient in the network stress, which has a maximum at the permeable surface. As Vomhoff [6] has demonstrated, web compaction starts in the fibre layers nearest the permeable surface(s) and progressively extends to the neighbouring layers.

As the fibre network becomes compacted, pressure builds up in the intra-fibre water until the pressure difference across the fibre wall surface is greater than the swelling pressure, and some of the intra-fibre water is driven out, as has been demonstrated by Carlsson et al. [8]. Since water flow is viscous, the structural pressure may be expected to be rate-dependent. Such rate-dependence was noted by Ceckler and Thompson [9] and was clearly demonstrated by Vomhoff's experiments [6].

Carlsson and co-workers have shown that a very significant amount of water may be pressed out of the fibre walls during wet pressing [10].

Wahlström [11] has suggested that intra-fibre water controls the compression behaviour of the fibre web and thereby the compressed web's density, permeability and solids content. The results of experimental studies support Wahlström's hypothesis [4,6]. Because of the importance of the flow out of the fibre wall on water removal, densification and density distribution, Wahlström [11,12] has pointed out that a proper mathematical description of wet pressing must take into account the force required to squeeze out the intra-fibre water. This is particularly important when evaluating the effect of shoe presses, which generate pressure pulses with sudden large changes in compression rate.

A number of quantitative models of wet pressing have been proposed in the literature, and a review of the work published before 1990 is available in [13]. New models have been proposed later by Kataja et al. [14,15], Bloch [16,17] and Riepen [18]. None of the published models include the rate-dependence of the structural pressure associated with the flow resistance of the intra-fibre water.

This paper presents a hydrodynamic model of wet pressing (at ambient or high temperatures) that takes into account the flow resistance of the intra-fibre water and can therefore be used to study web densification and dewatering. This has been achieved by the incorporation of a newly developed rheological model of wet fibre webs in wet pressing that includes the rate dependence of the structural pressure. The rheological model computes the structural pressure, which the hydrodynamic model then uses to determine the hydraulic pressure and the resulting flow.

Since the hydrodynamic model uses a numerical solver, it has been validated by a procedure for validating numerical codes recommended by NASA [19]. This has been done in three phases. First the rheological model was validated with the help of uniaxial compression experiments using a special laboratory device for measuring the structural pressure of a saturated wet fibre web [6]. It can predict the structural pressure of a wet fibre web resulting from a pressure pulse of arbitrary length and shape [20,21].

Then the predictive capability of the hydrodynamic model for wet pressing at ambient temperatures has been studied with the help of data from the third press of STFI's experimental paper machine, EuroFEX. The shape of the pressure pulse varied considerably in the range of operating cases covered in this study. The model gives good predictions over a wide range of grammages, machine speeds and loads. The prediction capability of the model is quite adequate for most engineering applications [22].

A number of high-temperature pressing processes have been envisaged, for example pressing with a heated roll [23,24,25]. Bloch [16] has proposed a model for high temperature pressing; Ramaswamy and Lindsay [26] have

compared two models developed in the United States, and Riepen [18] has presented simulation results.

In the final validation phase, we have studied the predictive capability of the hydrodynamic model we propose for wet pressing at high temperatures, with the help of a new set of data from the third press of EuroFEX. The data cover a range of press roll temperatures (25°C–230°C) and linear loads. The predictive capability of the model is quite good within the range of temperatures and linear loads studied.

The hydrodynamic model can simulate changes in the solids content and structural properties of the fibre web as it passes through a press nip. Once it has been calibrated, the model can predict the effects of changes in operating variables (such as hot roll temperature, peak pressure, pressure pulse shape or machine speed), the state of the ingoing web (e.g. the ingoing solids content, permeability or rheology) or felt properties. The model can calculate the variations in solid content and density in the thickness direction that often result from pressing events.

HYDRODYNAMIC MODEL

The model proposed is general in the sense that it can predict changes in the state of the fibre web due to a pressure pulse of arbitrary shape, under a wide range of saturation and temperature conditions. For example, the effect of a heated press roll can be taken into account. It can be applied to a variety of different wet pressing equipment (a roll press nip, an extended press nip or any device for laboratory wet pressing). In felted presses, the felt is included in the model. The rolls in a roll press, and the press shoe and belt in an extended press nip, are included as boundary conditions for the total force and pressures at the boundaries of the fibre web and felt(s).

Continuity equations

We treat the flow in a press nip as a two-phase flow in a deformable porous medium under a compression – decompression cycle. The continuity equations describe species mass and heat conservation:

$$\frac{\partial c^{\alpha}}{\partial t} + \nabla \cdot \mathbf{j}^{\alpha} = \Sigma^{\alpha} \tag{1}$$

where c^{α} is the concentration of $\alpha = \{s, w, a, v, U, V\}$ = {solid material, water,

air, water vapour, total internal energy, internal energy of the gas}, ∇ is the divergence operator, $\mathbf{j}^{\alpha}$ is the flux of α and Σ^{α} is the net creation of α per unit volume. Here we make no distinction between extra-fibre water and free intra-fibre water. The water bound to the cellulose fibres is here assumed to be constant and is included in the solid material. The source terms, Σ^{α}, contain the mass and energy transfer caused by evaporation and condensation.

Darcy's law and permeability

We assume that, in the fibre web and in the felt, the transport resistances of the fluids are linear functions of the differences between the fluid and solid velocities, which is equivalent to a postulation of Darcy's law:

$$\mathbf{u}^{\alpha} = -\frac{\mathbf{K}^{\alpha}}{\mu^{\alpha}(T)}\nabla p^{\alpha} \tag{2}$$

where $\alpha = \{w, g\} = \{$water, gas (air and water vapour)$\}$, $\mathbf{u}^{\alpha}$ is the Darcy velocity, which is defined as the flow of α per unit area. $\mathbf{K}^{\alpha}$ is the permeability matrix, μ^{α} is the fluid viscosity, T is the absolute temperature and p^{α} is the pressure in the fluid. The gas viscosity is estimated from the viscosities of air and water vapour:

$$\mu^{g} = x^{\alpha}\mu^{\alpha} + \mathrm{x}^{\mathrm{v}}\mu^{v} \tag{3}$$

where x^{α} and x^{v} are the molar fractions of air and water vapour in the gas. Here material coordinates are chosen as the frame of reference. This is equivalent to a frame of reference fixed in the undeformed fibre web. The mass flux vectors can then be written as a product of the densities and the Darcy velocities:

$$\mathbf{j}^{\beta} = \rho^{\beta}\mathbf{u}^{\alpha} \tag{4}$$

where $\beta = \{w, a, v\}$. The concentrations can be expressed as a product of the fluid densities ρ^{β} and the specific porosities n^{β}:

$$c^{\beta} = \rho^{\beta}n^{\beta} \tag{5}$$

where the specific porosity is defined as the pore volume occupied by species β divided by the total volume. The continuity equations (1) can then be written in the form:

$$\frac{\partial(\rho^{\beta} n^{\beta})}{\partial t} + \nabla \cdot (\rho^{\beta} \mathbf{u}^{\alpha}) = \Sigma^{\beta} \tag{6}$$

It is assumed that the permeability can be written as the product of a relative permeability function and an absolute permeability tensor:

$$\mathbf{K}^{\alpha} = k^{\alpha}(s) \cdot \mathbf{K}(n) \tag{7}$$

where k^{α} is the relative permeability, $\mathbf{K}$ is the absolute permeability, s is the reduced saturation (fraction of pore volume occupied by the liquid, excluding the volume occupied by the bound water) and n is the porosity (pore volume divided by the total volume). For the relative permeabilities, the estimation of Michaels [27] has been used, here as a function of the reduced saturation:

$$k^{g} = (1 + 3s)(1 - s)^3 \tag{8a}$$

$$k^{w} = s^4 \tag{8b}$$

The absolute permeability is assumed to be isotropic and to depend exponentially on the porosity:

$$\mathbf{K} = K_0 e^{an} \cdot \mathbf{I} \tag{9}$$

where K_0 and a are parameters and $\mathbf{I}$ is the identity matrix. In the general anisotropic case each component of the permeability tensor is a separate function of porosity. This case can also be handled by the model.

Capillary pressure

The treatment of the capillary forces follows the model presented by Bloch [16]. The water fills the smallest pores of the fibre web. We assume that the size of the pores can be described by a density function f for the hydraulic diameter. The density function is defined so that $\int_0^d f(u)du$ is the volume fraction of pores with a hydraulic diameter less than or equal to d. It is then assumed that all the pores with a diameter less than a critical diameter d_c are filled with liquid. The critical diameter can be defined implicitly as a function of saturation, s, by:

$$s = \int_0^{d_c} f(u)du \tag{10}$$

In the model, we assume that hydraulic diameters are distributed according to the Erlang function:

$$f(d) = \frac{(d/b)e^{-d/b}}{d\Gamma(c)} \tag{11}$$

where b is a scale parameter, c is a shape parameter, Γ is the gamma function and d is the hydraulic diameter.

For porous materials with a mean hydraulic diameter d_c, an equation for the capillary pressure can be derived from the equation of Young and Laplace [28]:

$$p_c(s) = \frac{4\gamma \cos(\theta)}{d_c} \tag{12}$$

where γ is the surface tension of the liquid and θ is the contact angle of the liquid-solid-gas line.

Force balance

Neglecting the shear forces in the fluids and the inertial terms, the sum of the loads supported by the fibres and the fluids must equal the applied total load:

$$p_t = -\sigma_s + \phi \cdot p_h \tag{13}$$

where p_t is total applied pressure, σ_s is the structural stress, defined as the fibre force in the positive z-direction divided by the total area of the surface of the volume element perpendicular to the z-axis, p_h is the pressure of the fluid and ϕ is a factor introduced by Biot [29]. The value of ϕ should lie between the porosity and unity. Both the hydraulic and the structural pressures are functions of the deformation of the fibre web and felt. When the fluid is unsaturated, the hydraulic pressure can be defined through the saturation and the pressures of the liquid and gas $p_h = s \cdot p_1 + (1 - s) \cdot p_g$.

The factor ϕ has been investigated by Kataja et al. [30] for blotting paper and nylon felt. They showed that it is equivalent to the effective areal porosity and can be written as $\phi = C + (1\text{-}C)n_a$ where C is a factor describing the influence of the hydraulic pressure on the structural stress and n_a is the areal porosity, here assumed to be equal to the volumetric porosity. Kataja et al. derived a linear relationship between C and the structural stress. This linear relationship could not be used in our model because it resulted in unreasonably low effective areal porosities for high structural stresses. Data from their experiments suggest that the factor C has a constant value of about 0.55 for

high structural stresses. This behaviour was introduced into the model by an exponential relationship for C:

$$C = 1 - D\left[1 - \exp\left(\frac{\sigma_s}{\sigma_k}\right)\right] \tag{14}$$

where $D = 0.46$ and $\sigma_k = 3.6$ MPa are parameters calibrated from the data published by Kataja et al.

Fibre web rheology

The equation for the plastic strain rate follows the model suggested by Lobosco and Kaul [20], here modified to incorporate the temperature-dependence of the strain rate:

$$\frac{d\varepsilon^{pl}}{dt} = \begin{cases} 0 & \text{for } F \le 0 \\ G(T)\cdot\Psi\cdot\sinh\left(B\dfrac{T_0}{T}F\right) & \text{for } F > 0 \end{cases} \tag{15a}$$

$$G(T) = -G_0\frac{T}{T_0}\exp[-G_x T_b(1/T - 1/T_0)] \tag{15b}$$

where ε^{pl} is the plastic strain, T_0 is a reference temperature (296.15 K), T_b is the boiling temperature of water at atmospheric pressure, $F = \sigma_s/\sigma_y - 1$ is the over-stress and σ_y is a hardening curve for the plastic strain. Lobosco and Kaul [21] have also investigated the temperature dependence of the plastic strain rate. Equations 15a,b fit well to the equation suggested by Lobosco and Kaul for low values of the over-stress and for temperatures in the range from 23 to 80 °C. Equations 15a,b are analogous to the equation of flow for a viscous fluid derived by Eyring et. al. [31], except for the factor Ψ. In this analogy, the strain rate plays the role of the mean velocity gradient and the over-stress is proportional to the shear stress. The parameter G can be interpreted as an inverse viscosity and the factor Ψ as the influence of the changing pore size distribution of the fibre walls on the mean velocity gradient. The parameters G_0, G_x and B have been determined by tuning Equations 15a,b to data from Lobosco and Kaul [21] for 23, 50 and 80 °C.

The function Ψ has been chosen by Lobosco and Kaul to fit experimental data:

$$\Psi = \left[\left(\frac{\sigma_y(\varepsilon^{pl}) - \sigma_y(\varepsilon^{pl}_{ref})}{\sigma_y(\varepsilon^{pl}_{ref})}\right)^2 + 1\right]^m \tag{16}$$

where ε^{pl}_{ref} is a reference plastic strain and m is a material parameter.

In this model, we have used a hardening curve function proposed by Kataja et al. [15]:

$$\sigma_y(\varepsilon^{pl}, T) = -E\frac{1-\exp(\varepsilon^{pl})}{\hat{c}(T)-[1-\exp(\varepsilon^{pl})]} \tag{17}$$

here slightly modified to be used with the plastic strain as an argument and with a logarithmic definition of the strain. E is a parameter and $\hat{c}$ is the maximum compression assuming that the cellulose and the bound water are incompressible. Stamm and Loughborough [32] have shown that the fibre saturation point of wood changes linearly with temperature in the range from 20 to 100 °C. The mechanism behind this is assumed to account also for the temperature-dependence of the bound water content. It is then reasonable to believe that the bound water content should be a linear function of temperature. Further, it is assumed that the observed shifts of the experimental hardening curves towards higher deformation for higher temperatures depends only on the difference in the bound water content. With these assumptions and assuming that the pulp yield is about 45%, a corresponding fibre saturation point slope for wood versus temperature can be calculated, yielding a value of 0.097%/°C. This is in very good agreement with the value 0.1%/°C published by Stamm and Loughborough [32].

For the elastic part of the strain, we use the equation given by Lobosco and Kaul [20], here solved for the structural stress σ_s:

$$\sigma_s = 3E_{el}\left[1-\exp\left(\frac{1+e_0}{\kappa}(1-\exp(\varepsilon^{el}))\right)\right] \tag{18}$$

where e_0 is the initial void ratio, $\varepsilon^{el} = \varepsilon - \varepsilon^{pl}$ is the elastic strain, and p_t and k are material parameters.

We have chosen to model the felt as a purely non-linear elastic material, described by Equation 18, using suitable values for the material parameters.

Evaporation and condensation

When heat is transferred from the roll to the fibre web, the water in the pore space will evaporate or vapour will condense, depending on the temperature and pressure of the water and the vapour. Evaporation is a fast process, and unless there is a heat and mass transfer resistance, it should be instantaneous in comparison to the time scales relevant in wet pressing. For the water present in the fibre walls, such a resistance can be expected, as the heat must

be conducted through the pores with a flow of vapour in the reverse direction and with a lower temperature than in the bulk of the gas. The same type of resistance can be expected for condensation, but with a different rate because vapour can condense both on the water surface and on the cellulose. The rates of evaporation and condensation are assumed to be proportional to the difference between the partial pressure of the saturated vapour at the temperature of the water-fibre mixture and the molar fraction of the vapour in the bulk of the gas:

$$\Sigma^v = -\Sigma^w = \Lambda\left(\frac{p_s}{p_g} - x^v\right) \tag{19}$$

where Σ^v is the evaporation rate per unit volume (also the source term for the continuity equation of water vapour), Λ is a parameter that depends on both the mass transfer coefficient and the interfacial area per unit volume, p_s is the saturation pressure (a function of temperature), p_g is the gas pressure, and x^v is the molar fraction of vapour in the gas.

Heat transfer

Heat is transported through the roll by conduction, and through the paper and the felt by convection and conduction. The gas phase can gain or loose mass and heat by evaporation or condensation. The total internal energy is not changed by evaporation or condensation. The flux of internal energy is the sum of convective and conductive fluxes:

$$\mathbf{j}^V = H^g\mathbf{u}^g - \lambda^g(n^a + n^v)\,\nabla T^g \tag{20a}$$

$$\mathbf{j}^U = H^w\mathbf{u}^w - \lambda^s n^s \nabla T - \lambda^w n^w \nabla T + \mathbf{j}^V \tag{20b}$$

$$\mathbf{j}^r = -\lambda^r \nabla T^r \tag{20c}$$

where $\{V, U, r\} = \{$ internal energy of the gas, total internal energy, roll$\}$, H is the enthalpy per unit volume of the fluid, λ^g, λ^s *and* λ^w are the thermal conductivities, and λ^g is calculated from the pure thermal conductivities of air and water vapour and from the molar fractions of the gas. The roll is covered with a steel belt with two layers of coating. The steel and the coatings have different thermal properties. Thus, the thermal conductivity of the roll is a function of the distance from the roll/paper interface.

Heat is also transferred from the gas to the water and to the fibre wall

by conduction. The transfer rate is assumed to be proportional to the temperature difference:

$$h_g = \eta(T_g - T) \tag{21}$$

where h_g is the heat transfer rate per unit volume and η is a parameter that depends on both the heat transfer coefficient and the interfacial area per unit volume. The parameter η can be estimated from a mass and heat transfer analogy [33]:

$$\frac{\eta}{\Lambda} = c_{pv} Le^{\frac{2}{3}} \tag{22}$$

where c_{pv} is the heat capacity of the vapour at the film temperature $(T_g + T)/2$. *Le* is the Lewis-number of the vapour, which is defined as the ratio of the thermal and mass diffusivities.

Evaporation also transfers heat from the water to the gas. This heat transfer rate is proportional to the rate of evaporation. The source term of the internal energy of the gas is the sum of these two transfer rates:

$$\Sigma^g = U^g - h_g \tag{23}$$

Initial and boundary conditions

For high temperature pressing, seven coupled equations have to be solved to calculate the flow and deformation in the wet fibre web and felt: the continuity equations for water, air, water vapour, total internal energy and the internal energy of the gas Equation 1, – five time-dependent partial differential equations (PDEs) –, the total pressure balance Equation 13, – an algebraic equation –, and the viscoplastic flow Equation 15a, – an ordinary differential equation (ODE). The five PDEs are parabolic as the highest time derivative is of the first order. The space derivatives are of the second order. The press roll is treated as a separate object; one PDE for the internal energy has to be solved.

The PDEs and the ODE need initial conditions. In the fibre web and in the felt, the PDEs need five conditions on each boundary. The initial and boundary conditions have to be consistent with the algebraic equation. As the frame of reference moves with the fibre web, the boundary conditions will change, depending on whether or not the fibre web and felt are in contact with the roll and belt. In our formulation, the condition for the total pressure appears as a

time-dependent term, driving the dynamics of the system. The duration of this pressure pulse depends on the length of the press nip and on the machine speed. The length of the press nip depends on the applied load and on the material properties of the fibre web and felt in a complicated way. A sensitivity analysis has shown that the final solids content of the fibre web is not sensitive to variations in the press nip length. In our model, we have assumed that the length is a constant that can be determined from the geometry of the nip.

Initial conditions have to be set regarding the water, air, and water vapour concentrations, the internal energies, and the plastic deformation everywhere in the fibre web and in the felt. The water concentration is calculated from the measured initial solids content, the air concentration from the estimated saturation, the vapour concentration from the initial temperature and the assumed relative humidity of the air, and the internal energies from the initial temperature. The initial plastic deformation is zero. The initial gradients are assumed to be zero. This is not strictly in agreement with the algebraic equation, because capillarity introduces an initial transient in the saturation, a pressure gradient and a plastic deformation. However, a sensitivity analysis has shown that this effect is negligible.

The boundary conditions are different for different types of pressing equipment. Here we give appropriate conditions for the third press nip in EuroFex, which is an extended press nip (Figure 1). The boundaries of the model can then be divided into eight parts with potentially different conditions, as shown in Figure 2:

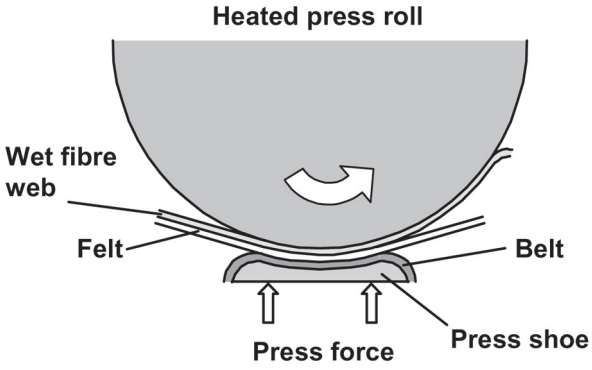

Figure 1 The third press nip on Euro-FEX is an extended press nip. Both the wet fibre web and the felt are included in the model.

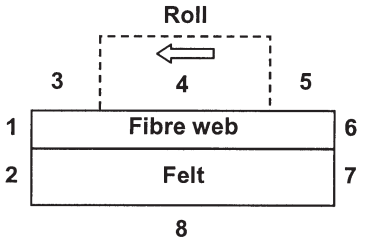

Figure 2 The computational domain of the model is fixed in the undeformed frame of reference. The roll acts as a moving boundary condition.

1 The initial fibre web boundary.
2 The initial felt boundary.
3 The uncompressed fibre web – atmosphere boundary.
4 The fibre web – roll boundary.
5 The compressed fibre web – atmosphere boundary.
6 The final compressed fibre web boundary.
7 The final compressed felt boundary.
8 The felt – belt boundary.

The boundaries 1, 2, 6 and 7 are similar because:

– The equations for the fibre web and the felt are similar; the only difference is in the material properties.
– There is no preferred direction in the equations. The displacement of the fibre web and felt relative to the paper machine enters the model through the time- and position-dependent applied pressure.

If these boundaries are set sufficiently far from the press nip, it is reasonable to assume that natural boundary conditions can be applied and that the flows of liquid gas and heat through these boundaries are zero.

The boundaries 3 and 5 are physically similar and should have the same conditions. They are permeable to gas and liquid. We have assumed that the gas pressure at these boundaries is atmospheric. We have also assumed that no water is present outside these boundaries and that water cannot therefore enter through the boundaries. Application of the definition of capillary pressure gives the boundary condition for the liquid pressure $p_l = p_c(s_b)$ where s_b is the saturation at the boundary calculated by the model. This is equivalent to a zero saturation gradient at the boundary. The water vapour concentration is assumed to be the same as in the ambient air. The conditions for the internal energies are calculated from the ambient temperature and pressure.

The boundary 4 is impermeable and the flows through the boundary are therefore set to zero. Through Darcy's law, this is equivalent to vanishing gradients of both liquid and gas pressure. The heat flow through the boundary is continuous.

As the belt is grooved, water and air can leave the felt at boundary 8 during compression. When the nip opens, the felt will expand due to its elasticity and some gas or liquid has to flow into the felt. For unsaturated felts the saturation is lowest at the belt side and we assume that the small amount of water entering the felt from the belt can be neglected. Thus, the conditions for boundary 8 are assumed to be the same as for boundaries 3 and 5.

The roll is heated with an induction heater before it makes contact with the fibre web. The different layers of the roll have different thermal and electrical properties. There is therefore an initial radial temperature gradient in the roll. It is assumed that this gradient has levelled out before the roll makes contact with the fibre web. Thus, the roll has a constant temperature along the radius at the contact point. Far from the roll – fibre web boundary and at the point where the roll and fibre web separate, the temperature gradient is assumed to be zero.

Simplifications

The geometry and nature of the press nips considered justify some assumptions that simplify the model. The variation in the length of the press nip is neglected. We also neglect the in-plane deformation and the fluid flow in the cross machine direction.

In the applications presented here the effects of capillary pressure both in the fibre web and in the felt have been neglected. This also implies that the liquid and gas pressures are assumed to be equal. Further, we have assumed that the amount of water transferred to the fibre web by separation rewetting depends only on the total area of the fibre web that has been in contact with the felt and is thus independent of the material properties, grammage and pressing event. It can then be given as a constant amount per unit area.

Discretisation

We have discretised the continuity equations by integration over finite volumes in the original undeformed reference system. This yields a system of ordinary differential equations for the mass and heat conservation and plastic strain rate. The pressure balance equation yields a system of algebraic equations. The resulting differential algebraic state equations are integrated with a solver for stiff differential-algebraic equations in MATLAB® [34].

In calculations using the model, the number of volumes used in the machine direction was one. Martinez [35] has shown analytically that the velocity difference between the fluid and the fibre web is small in comparison to the transversal velocity for roll presses under normal conditions. For the low temperature application, the number of volumes in the z-direction was 10 for the fibre web and 5 for the felt. A sensitivity analysis has shown that these numbers of volumes are adequate.

For the high temperature application, it is necessary to divide the fibre web into more volumes because of the high temperature gradients near the initial contact point. Comparison of final solids content values for different numbers of volumes has shown that 50 is an adequate number. For the roll, it is necessary to use 30 divisions. The size of the volumes decrease towards the roll – fibre web interface, both in the roll and in the fibre web.

PILOT PAPER MACHINE TRIALS

In order to evaluate the predictive capability of the proposed model, we have collected data from the third press nip of the EuroFEX experimental paper machine at STFI. The pulp used was a bleached kraft beaten to 25 SR. After the wire section, the fibre web is fed into the first press, a double-felted roll press. The second and third press nips on EuroFEX are extended nips with the press shoes on opposite sides of the fibre web. Both the second and third press nip rolls can be heated to 350°C. In the trials presented here, the second press nip roll was always cold.

Ambient temperatures

A series of seven trials were conducted, each trial having a particular combination of grammage and machine speed (see Table 1) and with both extended press rolls at ambient temperature. The same pulp (bleached softwood kraft pulp) was used in all the trials and the linear loads on the first and second press nips were kept constant at 60 and 200 kN/ m. In each trial, the linear load of the third press was varied from 200 to 1000 kN/m. Samples of the fibre web were collected before the first and third nips, and after the third press nip. The grammage and solids contents of these samples were determined (see Table 2).

The following values for the material properties of the fibre web were used in the calculations:

- Rheology: $G_0 = 146\ s^{-1}$, $m = -0.688$, $B = 0.567$, $G_x = 6.61$, $E = 136$ MPa, $c_0 = n_0 - 0.05$, n_0 is the initial porosity, $\varepsilon_{ref}^{pl} = -0.1$, $p_t = 0.02$ MPa, $k = 0.1$
- Permeability: $K_0 = 1.0 \cdot 10^{-22}\ m^2$, $a = 20.6$
- Density of cellulose: 1549 kg/m^3
- Bound water: 0.33 kg/kg fibre
- Rewetting: 4 g/m^2

Table 1 Grammage, machine speed and measured web solids content before the third press for the seven trials on the EuroFEX experimental paper machine.

Trial No.	Grammage g/m^2	Machine speed m/min	Solids content before the third nip %
1	80	300	37.5
2	80	450	36.7
3	100	300	37.8
4	100	450	36.0
5	100	600	34.7
6	120	300	36.7
7	120	450	34.9

Table 2 Measured solids content (%) after the third press nip. The values in bold type are used for calibration of the material properties. The values in italics are used to estimate the initial degree of saturation and thickness of the web (600 kN/m). The other cases were used to test the predictive capability of the model.

Linear load kN/m	Trial No.						
	1	2	3	4	5	6	7
200	39.5	39.0	40.0	38.6	37.1	39.0	37.8
400	41.1	**40.6**	41.4	40.2	38.3	40.1	38.8
600	42.1	41.2	42.5	41.1	39.1	40.8	39.8
600	*42.1*	*41.2*	*42.1*	*40.6*	*39.1*	*41.1*	*39.5*
600	42.0	41.2	42.0	40.6	39.0	41.0	40.0
800	42.8	**42.0**	42.7	41.4	39.5	41.5	40.3
1000	43.6	42.4	43.2	41.8	40.1	42.0	40.7

The permeability data used are based on laboratory measurements on web samples taken from between the second and third presses of EuroFEX.

The values used for the felt parameters were:

– Rheology: $E = 0.6$ MPa, $c_0 = 0.2$
– Permeability: $K_0 = 1.53 \cdot 10^{-13}$ m^2, $a = 5.39$
– Density of fibres: 1140 kg/m^3
– Grammage: 1430 kg/m^2
– Initial thickness: 3 mm
– Initial moisture ratio: 0.3 kg/kg solids.

The initial porosity of the felt was calculated from the grammage and the density of the felt fibres. The initial degree of saturation of the felt was calculated from the measured moisture ratio, the initial thickness, the density of the felt fibres and the grammage.

As an experimentally determined hardening curve for the fibre web entering the third press nip was not available, a suitable value for the stiffness of the hardening curve had to be determined by calibration. Two operating cases (grammage 80 g/m^2, machine speed 450 m/min, linear loads 400 and 800 kN/m) were used to calibrate this parameter (E in Equation 17). In future applications, we intend to use values of hardening curves derived from laboratory experiments on webs of the same pulp, submitted to the same load history as in a paper machine, in order to reduce the need for calibration. That will also increase the reliability of the simulation results.

To determine the initial web thickness, the degree of saturation is needed. This parameter is difficult to measure on-line or from fibre web samples taken before the third press nip. It had to be determined by calibration. The saturation value cannot be expected to be constant when the machine speed or the grammage is changed. For each trial with different combinations of grammage and machine speed, one of the cases with linear load 600 kN/m was used to estimate of the initial degree of saturation. The remaining cases (used neither for calibration nor estimation) were used to test the ability of the model to predict the solids content of the fibre web at the exit of the nip.

High temperatures

A series of five trials with different temperatures on the third press nip were conducted, each trial having the same grammage and machine speed see Table 3. All other conditions and procedures for the sampling and determination of the solids content were the same as for the ambient temperature trials.

The value for the combined heat transfer and specific interface area parameter, Λ in Equation 19, and the initial degree of saturation had to be determined by calibration. The temperature-independent parameters were the same as in the ambient temperature trials. The parameters describing

Table 3 Measured solids content (%) before and after the third press nip at different linear loads and temperatures. The values in bold type are used for calibration of the material properties and the initial degree of saturation. The other values were used to test the predictive capability of the model (grammage 80 g/m^2, machine speed 450 m/min).

Roll temperature °C	Solids content before the nip %	Linear Load kN/m 200	400	600	800	1000
		Solids content after the nip				
25	39.2	**40.3**		42.6	43.3	**43.6**
50	39.0	40.1		43.0	43.8	44.3
85	39.1	41.0		44.1	44.3	45.2
200	38.9	**43.1**	46.2	47.2	48.5	**49.2**
230	39.2	44.1	47.1	48.1	50.0	50.8

the temperature-dependences were taken from experimental data or from the literature. All other parameters were the same as in the ambient temperature trials.

The following values were used for the parameters specific to the high temperature trials:

– Evaporation: $\Lambda = 4.99 \cdot 10^5$ kg/m^{3}s.
– Initial degree of saturation: 81.5%.

RESULTS AND DISCUSSION

Ambient temperature

Figure 3 present comparisons of the measured and predicted solids content after the third press. The model appears to give good predictions over a wide range of grammages, machine speeds and loads. It may be noted that the shape of the pressure pulse varies considerably in the range of operating cases covered in this study.

There are, however, significant discrepancies between measured and predicted values that may be due to experimental errors or prediction errors. Experimental errors may be due to errors in the measurement of solids content (before and after the third press) and/or to the variability of the process.

Some indication of the size of the experimental errors may be obtained by studying Table 2. Compare the web solids content after the third press for the three cases in each trial that have identical operating conditions (with linear

Table 4 The sensitivity of the web solids content after the third press to some important parameters (trial 4, load 1 000 kN/m). Sensitivity is here defined as the relative change in solids content divided by the relative change in the parameter, for a small positive relative change in the parameter (5%).

Solids content before the third nip	1.12
Water saturation	0.43
Parameter in the elastic equation (k)	0.17
Permeability equation exponent (a)	0.11
Density of cellulose	–0.07
Fraction of bound intra-fibre water	0.06
Linear load	0.06

load 600 kN/m). The values of the solids content for the same operating condition can differ by up to 0.5%-units.

We have tried to analyse the most significant sources of prediction error. Prediction error may be caused by error in the input data and/or by deficiencies in the model.

The effects of errors in the input data have been estimated by a sensitivity analysis, sensitivity being defined as the relative change in the solids content divided by the relative change in the parameter, for a small positive change. Table 4 presents the sensitivity of the predicted solids content (after the third press) to changes in those input parameters which the analysis has shown to be the most significant.

The model is most sensitive to errors in the measurement of solids content before the third nip. An analysis of continuous on line measurements indicates that the standard deviation of the ingoing solids content from the off-line laboratory measurements is 0.1–0.2 percentage points. Thus, measurement errors can explain most of the discrepancies between the measured and observed solids content after the third press, as indicated by the dashed lines in Figure 3. Since only two of the points in Figure 3 lie outside the 2σ-lines, we feel that the overall prediction capability of the model as regards solids content is quite adequate for most engineering applications.

The effects of simplifying assumptions, like the assumption of zero cross-machine direction flow and deformation, and discretisation errors have been shown to be negligible compared to the experimental error.

This model can give interesting information about the sequence of events in the nip provided that the material properties (i.e., the permeability and hardening curves) have been derived independently of the model (e.g., from laboratory test results). As Danielsson [36] has demonstrated, we cannot be sure that the model is simulating events in the nip accurately unless the

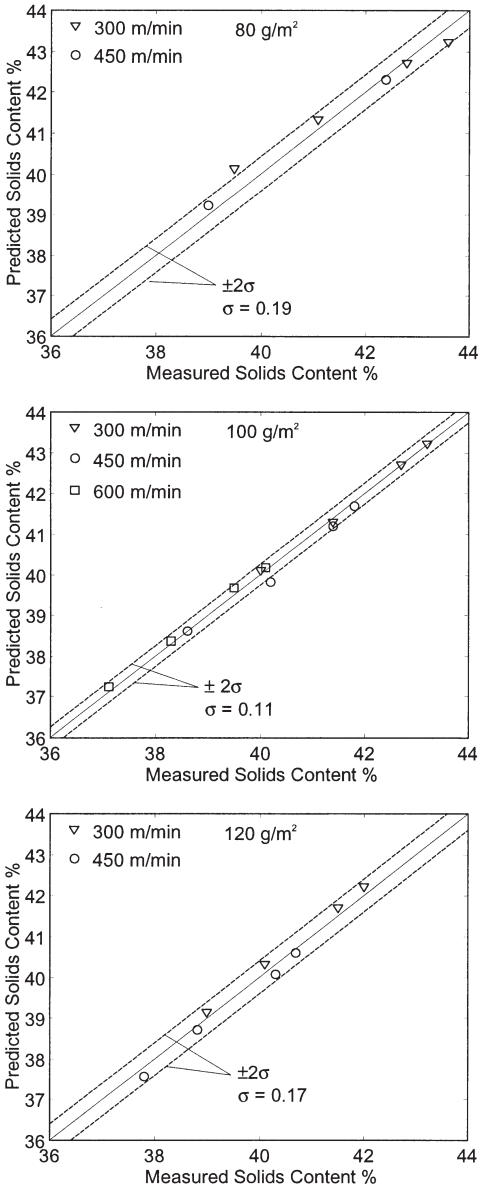

Figure 3 Predicted and measured solids content for different machine speeds and different grammages after pressing at different loads.

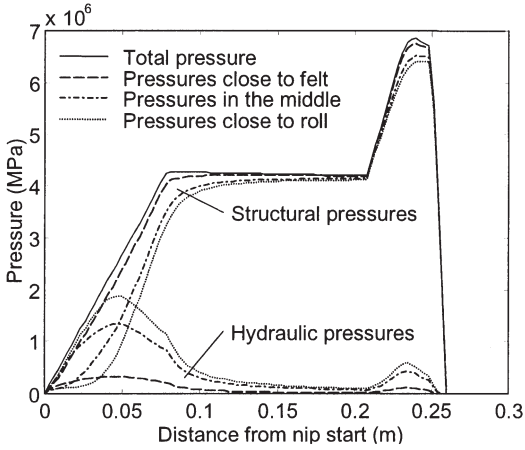

Figure 4 Calculated pressures along the third press nip of EuroFEX, at different levels in the wet fibre web (grammage 100 g/m^2, linear load 1000 kN/m, machine speed 450 m/min).

material properties have been derived independently of the model. Figure 4 shows how the local hydraulic and structural pressures (at different positions in web) vary inside the nip. Similar information can be obtained for a large number of local variables such as density, fluid velocity, permeability and degree of saturation.

High temperatures

The comparison between predicted and measured solids content for different roll temperatures and linear loads is shown in Figure 5. The agreement is satisfactory but the standard deviation of the discrepancies in Figure 5 is clearly greater than that for the discrepancies in Figure 3. Further, there are some systematic discrepancies in Figure 5 that should be noted. At low temperatures, when there is no evaporation, the model under-predicts the solids content. At high temperatures, when evaporation does occur, the model has a tendency to under-predict the increase in solids content with increasing linear load.

Since the model gives good predictions when the press roll is kept at ambient temperature, Figure 3, we conclude that the larger discrepancies in

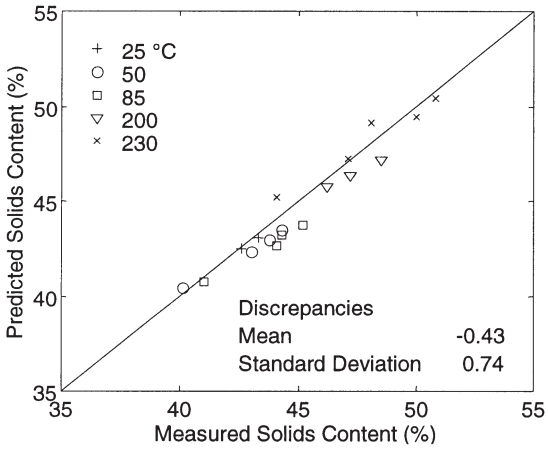

Figure 5 Predicted and measured solids content for different roll temperatures at different loads for a grammage of 80 g/m^2.

Figure 5 are related to the change in the press roll temperature. We believe this is mainly due to a combination of three sources of error. The first of these is the difficulty in obtaining a representative sample of the fibre web after the third press and accurately determining its solids content when the press roll temperature is high. At present we see no practical possibility of reducing this source of error.

A second possible source of error may be the hardening curve stiffness values used at high temperatures. The values used are based on extrapolation from measurements at lower temperatures, because the experimental determination of a hardening curve is extremely difficult at temperatures above 100°C. We believe that it is possible to reduce this source of error and we are working towards that goal.

A third significant source of error is the fact that while the model assumes that separation rewetting is the same in all cases, the actual separation rewetting is likely to be temperature dependent. Unfortunately we do not have any experimental data regarding the dependence of separation rewetting on temperature.

So far, we have not been able to check the model calculations of outgoing web thickness due to lack of reliable on-line measurements of ingoing and outgoing web thickness. The measurements need to be as close to the nip as possible, since the web starts expanding at the end of the nip. We have

attempted to develop on-line web thickness sensors, but that has proved to be very difficult. So we plan to check the thickness calculations with the help of data from laboratory experiments.

The results of the model simulations can give an insight into the mechanisms that are active in the nip. An interesting example concerns the model predictions of heat transport inside the fibre web. Figure 6 shows the evaporation and condensation rate profiles at two positions in the press nip. At mid-nip, there is a zone with a high evaporation rate close to the roll. This zone expands from the roll boundary into the web as the web moves within the nip and more heat is transferred into the web. At peak pressure, the evaporation rate is lower but the zone is broader. The vapour formed moves from this zone some distance away from the roll and condenses when it meets sufficiently cooler fibres. This vapour flow contributes to the total heat flow through the web, although conduction is the dominating mechanism for heat transport in most parts of the web.

Figure 7 shows that the hydraulic pressure close to the roll is higher at high than at low temperatures. The higher hydraulic pressure also leads to a higher dewatering because the pressure gradient and the flow in the z-direction are higher. The development of the web thickness through the press nip is almost the same for low and high temperatures Figure 8. This simulation example

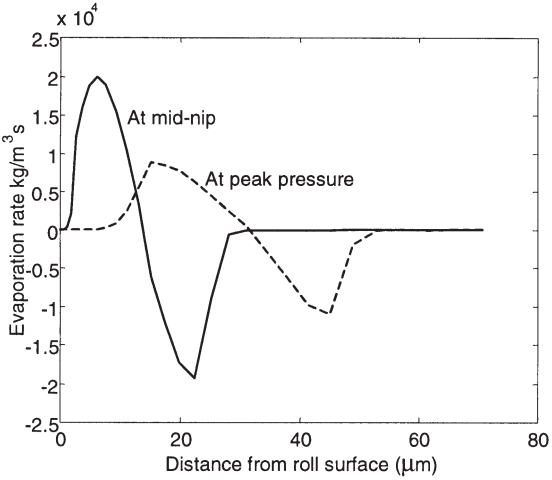

Figure 6 Calculated profiles of evaporation (+) and condensation (–) rates (grammage 80 g/m^2, linear load 1000 kN/m, machine speed 450 m/min, roll temperature 230°C).

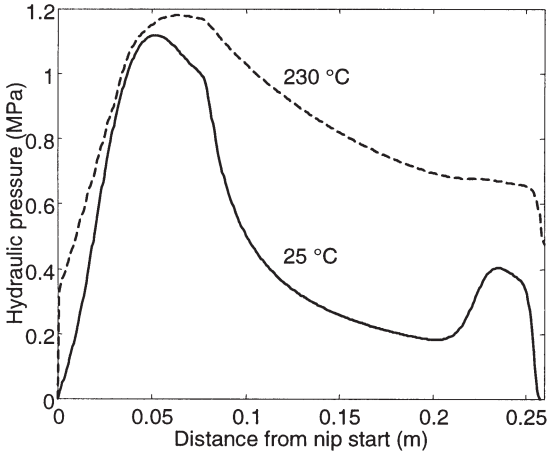

Figure 7 Calculated hydraulic pressure close to the roll for low and high temperature (grammage 80 g/m^2, linear load 1000 kN/m, machine speed 450 m/min).

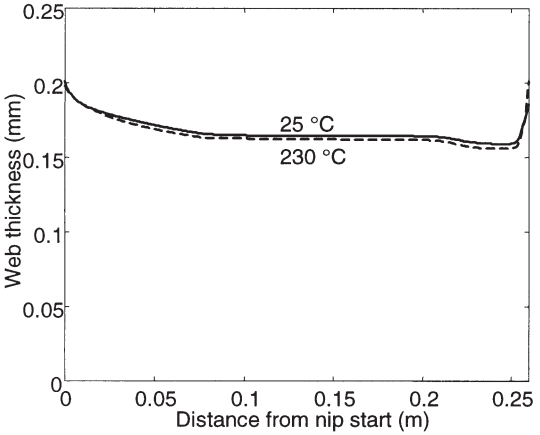

Figure 8 Calculated web thickness development for low and high temperature.

shows how high temperature pressing can result in higher solids content without any substantial lowering of the bulk.

The model assumes that mass-and heat-transfer resistances retard the evaporation and condensation processes in the fibre walls. It may be noted that if the mass transfer coefficient is increased to a high value, corresponding to local equilibrium in the fibre wall, the model becomes insensitive to load changes at constant high temperatures. This is because the hydraulic pressure is then completely determined by the temperature, wherever vapour is present. This is contrary to the observed sensitivity of the experimental results to load changes. We therefore conclude that there are significant mass and heat transfer resistances in the fibre web.

CONCLUSIONS

A hydrodynamic model of wet pressing by a press roll at both ambient and high temperatures has been presented that includes the rate-dependence of the fibre network stress and thus takes into account the flow resistance of the intra-fibre water. The model is general in the sense that it can predict changes in the state of the fibre web due to a pressure pulse of arbitrary shape, under a wide range of web saturation and temperature conditions. It can be applied to a variety of different wet pressing equipment (a roll press nip, an extended press nip or any device for laboratory wet pressing). The model can simulate changes in the solids content and structural properties of the fibre web as it passes through a press nip.

The predictive capability of the model has been studied with the help of data from the third press of a pilot paper machine. For wet pressing at ambient press roll temperatures, the model gives good predictions of solids content over wide ranges of machine speeds, grammages and linear loads. The prediction capability of the model regarding solids content is quite adequate for most engineering applications at ambient temperatures. A sensitivity analysis of the model at ambient temperatures indicates that the predicted outgoing solids content is influenced most by the solids content, water saturation and rheological properties of the ingoing web.

For high press roll temperatures the predictions are satisfactory over a wide range of press roll temperatures and linear loads, but some significant systematic discrepancies are observed. These predictions can probably be improved by using better estimates of the hardening curves at high temperatures. Once calibrated, the model can give considerable information about changes in the state of the web as it passes through the nip and some insight into the mechanisms that are active.

ACKNOWLEDGEMENTS

We are grateful to Professor Bo Norman for many illuminating discussions concerning the mechanisms active in pressing and to Dr. Jean-Francis Bloch for sharing with us his knowledge and insight regarding the modelling of wet pressing. We thank Dr. Jonas Funkquist for making available to us data from EuroFEX trials conducted by him. The work reported here was partially funded by the JOULE programme of the European community.

NOMENCLATURE

a	Exponent in the permeability/ porosity relationship
b	Scale factor in hydraulic diameter density function (m)
B	Parameter in the viscoplastic rheology
c	Shape factor in the hydraulic diameter function
c^{α}	Concentration of α (kg/m^3)
c_{pv}	Specific heat capacity of the vapour at the film temperature (J/kgK)
C	Hydraulic pressure influence factor
d	Hydraulic diameter (m)
d_c	Critical hydraulic diameter (m)
D	Parameter in the hydraulic pressure influence factor relationship
e_0	Initial voids ratio
E_{el}	Parameter in the elastic stress – strain function
f	Hydraulic diameter density function (m^{-1})
F	Over-stress
G_0	Parameter in the viscoplastic rheology (s^{-1})
G_x	Parameter in the viscoplastic rheology
h_g	Heat transfer rate from the gas to the solid and liquid (W/m^3)
H^g	Enthalpy of gas per unit volume (J/m^3)
H^w	Enthalpy of water per unit volume (J/m^3)
$\mathbf{j}^V$	Flux of internal energy in the gas (W/m^2)
$\mathbf{j}^U$	Total flux of internal energy (W/m^2)
$\mathbf{j}^r$	Flux of internal energy in the roll (W/m^2)
$\mathbf{j}^{\alpha}$	Flux vector of α (kg/m^{2}s)
k^{α}	Relative permeability for α
K_0	Parameter in the permeability/ porosity relationship (m^2)
$\mathbf{K}$	Absolute permeability (m^2)
$\mathbf{K}^{\alpha}$	Specific permeability matrix, gas or liquid (m^2)
Le	Lewis-number of water vapour
m	Parameter in the strain rate function

n	Porosity
n^{β}	Specific porosity of β, water air or water vapour
p^{α}	Gas or liquid pressure
p_s	Saturation pressure function
p_c	Capillary pressure (Pa)
p_t	Total applied pressure (Pa)
p_h	Hydraulic pressure (Pa)
s	Reduced saturation
t	Time (s)
T	Absolute temperature (K)
T^r	Temperature in the roll (K)
T_0	Reference temperature (K)
T_b	Boiling temperature of water at atmospheric pressure (K)
U^g	Heat transfer from water to gas by evaporation (W/m^3)
$\mathbf{u}^{\alpha}$	Darcy velocity vector (m/s)
x^{α}	Molar fraction of air or water vapour in the gas
α	Material index = { *s, w, a, v, U, V*} = {solid material, water, air, water vapour, total internal energy, internal energy of the gas}
Γ	The gamma function
γ	Surface tension of water (Pa/m)
∇	Divergence operator (m^{-1})
ε^{el}	Elastic strain
ε	Total strain
ε^{pl}_{ref}	Plastic reference strain
ε^{pl}	Plastic strain
η	Heat transfer parameter (W/m^{3}K)
θ	Contact angle (180°)
κ	Parameter in the elastic stress – strain function
Λ	Evaporation mass transfer parameter (kg/m^{3}s)
λ^g	Thermal conductivity of the gas (W/mK)
λ^s	Thermal conductivity of the fibre material (W/mK)
λ^w	Thermal conductivity of water (W/mK)
λ^r	Thermal conductivity of the roll (W/mK)
μ^{α}	Viscosity, gas or liquid (Pas)
ρ^{α}	Density of α (kg/m^3)
σ_k	Parameter in the hydraulic pressure influence factor relationship (Pa)
σ_s	Structural stress (Pa)
σ_y	Plastic yield stress
Σ^{α}	Net creation of α (kg/m^{2}s)
ϕ	Effective areal porosity

Ψ Factor in strain rate equation
Ω Strain rate function

REFERENCES

1. MacGregor, M.A., "Wet Pressing Research in 1989 – An Historical Perspective, Analysis, and Commentary", Transaction of 9th Fundamental Research Symposium, Cambridge, England, 511–586 (1989).
2. Szikla, Z., "On the Basic Mechanisms of Wet Pressing", PhD Thesis, Helsinki University of Technology, Helsinki (1992).
3. Burns, J.R., Lindsay, J.D., Connors, T.D., "Dynamic Measurements of Stratified Consolidation in a Press Nip", Proc. Tappi Eng. Conf., 899–916 (1992).
4. Laivins, G.V., Scallan, A.M., "Removal of Water from Pulps by Pressing, Part I: Inter-and Intra-wall Water", TAPPI Engineering Conf. (1993).
5. Ahlman, A.-K., "Development of a Laboratory Shoe Press and a Study of Separation Rewetting", Licentiate Thesis, Royal Institute of Technology, Division of Paper Technology, Stockholm (1997).
6. Vomhoff, H., "Dynamic compressibility of water saturated fibre networks and influence of local stress variations in wet pressing", Doctoral Thesis, Royal Institute of Technology, Department of Paper Technology, Stockholm (1998).
7. Maloney, T., "On the Pore Structure and Dewatering Properties of the Pulp Fiber Cell Wall", Acta Polythechnica Scandinavica, Chemical Technology Series No. 275 (2000).
8. Carlsson, G., Lindström, T., Söremark, C., "Expression of water from cellulosic fibres under compressive loading", BPB1F Transactions from the 6th Fundamental Research Symposium – Fiber-water interactions (2 Vols), Oxford, England (1977).
9. Ceckler, W.H., Thompson, E.V., "The University of Maine at Orono Wet Pressing Project: Final Report", U.S. Department of Energy, Washington, D.C., (1982).
10. Carlsson, G., "Some Fundamental Aspects of the Wet Pressing of Paper", Doctoral Thesis, Royal Institute of Technology, Department of Paper Technology, Stockholm, (1983).
11. Wahlström, P.B. (1990), "The Effect of Water in the Fibre Wall on Wet Pressing", Appita General Conference, Rotoroa, A21.1–A21.24.
12. Wahlström, P.B., "Pressing – the state of the art and future possibilities", Paper Technology, February 1991, 18–27 (1991).
13. El-Hosseiny, F., "Compression Behaviour of Press Felts and Wet Webs", *Nord. Pulp Pap. Res. J.*, **5**: 1, 28–32 (1990).
14. Kataja, M., Hiltunen, K., Talja R., Timonen, J., "A Hydrodynamical Model of Wet Pressing of Paper", TAPPI Eng. Conf., Boston, Sep. 14–17 1992, 403–424 (1992).
15. Kataja, M., Hiltunen, K., Timonen, J., "Flow of water and air in a compressible

porous medium. A model of wet pressing of paper", *J. Phys. D: Appl. Phys.*, **25**: (1992), 1053–1063 (1992).
16. Bloch, J.-F., "Transferts de Masse et de Chaleur dans les Milieux Poreux Deformables non Satures: Application au Pressage du Papier", Ph.D. Thesis, Institut National Polytechnique de Grenoble, Grenoble (1995).
17. Bloch, J.-F., Silvy, J., Roux, J.-C., Aurialt, J.-L., "Wet pressing of paper and filtration laws", Recueil de Conférences, 7th World Filtration Congress, Budapest, Vol I, 47–51 (1996).
18. Riepen, M., "An Inside View on Impulse Drying Phenomena by Modelling", *Tappi J.*, **83**: 10 (2000).
19. NASA, "Procedure And Criteria For Assessing CFD Code", NASA Tech Briefs, MFS-29972.
20. Lobosco, V., Kaul, V., "An elastic/viscoplastic model of the fibre network stress in wet pressing: Part I", accepted for publication in *Nord. Pulp Pap. Res. J*. (2001).
21. Lobosco, V., Kaul, V., "An elastic/viscoplastic model of the fibre network stress in wet pressing: Part 2 Accounting for pulp properties and web temperature", submitted to *Nord. Pulp Pap. Res. J*. (2001).
22. Gustafsson, J-E., Kaul, V., "A General Model of Deformation and Flow in Wet Fibre Webs under Compression", accepted for publication in *Nord. Pulp Pap. Res. J*. (2001).
23. Orloff, D.I., Phelan, P.M., Crouse J.W., "Impulse drying of board grades: pilot production trials", *Tappi J*, **83**: 9, 57 (2000).
24. Rigdahl, M., Bäckström M., Hedström C-G., Norman B., Kilian M., Talja R. "Impulse Technology on the EUROFEX Machine", *Tappi J*., **83**: 8 (2000).
25. Pikulik, I., Hamel, J. "The Effects of Shoe Pressing on The Properties of Wood-Containing Papers", *Tappi J*, **83**: 8 (2000).
26. Ramaswamy, S., Lindsay, D.L., "The role of vapor formation on high-intensity drying – description and comparison of two models", *Nord. Pulp Pap. Res. J*., **13**: 4, 299–309 (1998).
27. Wilder, J. E., "Paper Capillarity and Rewetting During Pressing", *Tappi J*., **51**: 2, 104–109 (1968).
28. Adamson, W.A., "Physical Chemistry of Surfaces", Wiley-Interscience, New York (1990).
29. Biot, M.A., "General Theory of Three-Dimensional Consolidation", *J. Appl. Phys.,* 12, p. 155–164 (1941).
30. Kataja, M., Kirmanen, J., Timonen, J., "Hydrostatic and Structural Pressure in Compressed Paper Webs and Press Felts", *Nord. Pulp Pap. Res. J*., **10**: 3, 162–166 (1995).
31. Bird, R.B., Stewart, W.E., Lightfoot, E.N., "Transport Phenomena", Wiley International Edition (1960).
32. Stamm, A.J., Loughborough W.K., "Thermodynamics of the Swelling Wood", *The Journal of Physical Chemistry*, **39**: 1 (1934).
33. Beek, W.J., Muttzall, K.M.K., "Transport Phenomena", Wiley-Interscience, London (1975).

34. Shampine, L.F., Reichelt, M.W. "The MATLAB ODE Suite", *SIAM Journal on Scientific Computing*, **18**:1, 1997 (1997).
35. Martinez, D.M., "An Estimate of the In-Plane Velocity Difference Between the Fibres and Water During Wet Pressing: The Saturated Case", *Journal of Pulp and Paper Science*, **25** 12, pp. 403–409 (1999).
36. Danielsson, K., "Identification of a Wet Pressing Model for a Research Paper Machine", Licentiate Thesis, Royal Institute of Technology, Department of Signals, Sensors and Systems, Stockholm (1998).

Transcription of Discussion

DENSIFICATION AND DEWATERING IN HIGH TEMPERATURE WET PRESSING

Jan-Erik Gustafsson, Vikram Kaul and Vinicius Lobosco
STFI

Ref. 13. should be: El-Hosseini F., "Mathematical Modelling of Wet Pressing of Paper", *Nord. Pulp Paper Res. J.*, **6**: 1. 30–34 (1991)

The figure below was used in the discussion but not shown in the paper preprint.

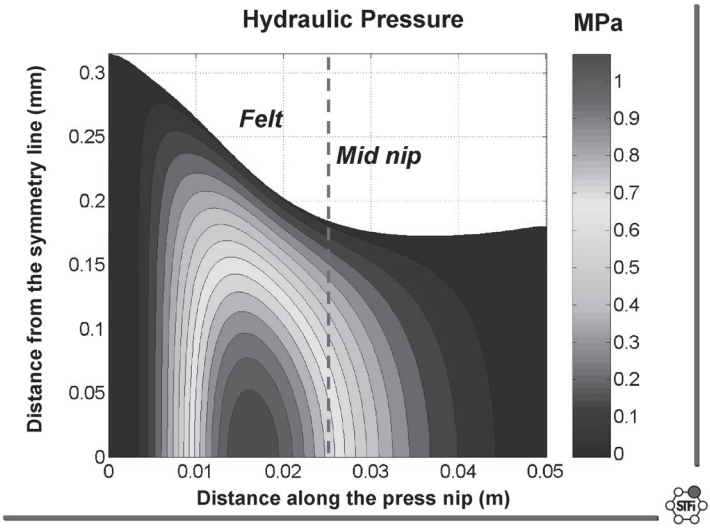

Figure 1 Calculated hydraulic pressure in a double felted roll press nip (due to symmetry only the upper part of the fibre web is show). Lineal load 60 kN/m, grammage 100 g/m^2, machine speed 450 m/min.

Discussion

Ron Crotogino Paprican

At the beginning of your talk, you stated the assumption that there was no flow of water in the machine direction in the press nip. However, in your slide [Figure 1 above] there appears to be a higher gradient of hydraulic pressure in the MD than in the CD. How can this be justified?

Jan-Erik Gustafsson

What I should have mentioned in my talk is that the figure in the slide is scaled differently in the two directions and the gradient is, in fact, much higher in the z-direction.